Engineering Applications of Artificial Intelligence 100 (2021) 104206

Contents lists available at ScienceDirect

Engineering Applications of Artificial Intelligence

journal homepage: www.elsevier.com/locate/engappai

A temporal LASSO regression model for the emergency forecasting of the suspended sediment concentrations in coastal oceans: Accuracy and interpretability

Shaotong Zhang [a,c,*], Jinran Wu [b,d,*], Yonggang Jia [a,*], You-Gan Wang [b,d], Yaqi Zhang [c], Qibin Duan [b,d]

[a] Key Laboratory of Shandong Province for Marine Environment and Geological Engineering, College of Environmental Science and Engineering, Ocean University of China, Qingdao 266100, China
[b] School of Mathematical Sciences, Queensland University of Technology, Brisbane 4001, Australia
[c] Key Laboratory for Submarine Geosciences and Prospecting Technology, Ministry of Education, College of Marine Geosciences, Ocean University of China, Qingdao 266100, China
[d] ARC Centre of Excellence for Mathematical and Statistical Frontiers, Queensland University of Technology, Brisbane 4001, Australia

ARTICLE INFO

Keywords:
Machine learning
Empirical mode decomposition
Spectrum analysis
Sediment resuspension
Tidal advection
Static settling

ABSTRACT

In situ observations of suspended sediment concentration (SSC) and hydrodynamics were conducted in the subaqueous Yellow River Delta, China. With the dataset, a new least absolute shrinkage and selection operator (LASSO) regression model with temporal autocorrelation incorporated (temporal LASSO) is proposed for SSC prediction and mechanism investigation in coastal oceans. The model is concise and practical, effectively shrinking the interrelated variables into representative ones, while also achieving one-hour ahead forecasting with both higher accuracy and better interpretability than other data-driven methods. The model interpretability is further validated with direct data analysis from a physical perspective. Specifically, Empirical Mode Decomposition is employed to decouple the measured SSC into intrinsic mode functions (IMFs) and a residual. The periods of each subseries estimated from both zero-crossing and spectrum analysis show that IMF_1 physically corresponds to the sediment resuspension by M4 tidal currents, IMF_2 is the M2 tidal advection, IMF_3-IMF_5 are the resuspension by wind waves, IMF_6 is the spring–neap tidal pumping of sediments. The contributions estimated with the ratio of variance are 12 %, 14 %, 63 %, and 10 %, respectively, over the observation period. The residual is the seasonal variations which can be taken as the background SSC thus not included for variance contribution. Waves make the dominant contribution which verifies the rationality of the LASSO shrinkage and confirms the model interpretability. The temporal LASSO model is shown to be a potential tool for emergency forecasting and mechanism explanation of SSC to benefit ocean environmental engineering management.

1. Introduction

The suspended sediment concentration (SSC) in rivers and oceans is one of the most important factors that determine the water quality as it affects the light transmittance and thus the photosynthesis in aquaculture (Lloyd, 1987; Zang et al., 2020). The SSC in coastal oceans is also very geologically significant, as the transport of SSC determines the regional sediment budget and ultimately influences the long-term evolution of coastlines and beaches (Lambrechts et al., 2010). Therefore, obtaining adequate SSC information is a goal that has been pursued by site engineers and researchers in environmental, hydraulic, and coastal engineering.

Traditionally, the SSC was directly determined by the physical collection of water samples and subsequent analysis in the laboratory (e.g., Nielsen, 1984), but this is a survey method that cannot be used for prediction. However, predictions are much more important than surveys for engineering purposes. In particular, with marine ranching becoming more popular in recent years, even a short-period ahead forecast (Taormina et al., 2012; Lahmiri, 2015) of the SSC is extremely beneficial in the emergency management of ocean environmental engineering issues.

Regarding a predictive model, extensive efforts have been devoted in the past century to developing process-based models using physical approaches. As the SSC at a certain elevation in the water column is

* Corresponding authors.
E-mail addresses: shaotong@ouc.edu.cn (S. Zhang), jinran.wu@hdr.qut.edu.au (J. Wu), yonggang@ouc.edu.cn (Y. Jia).

https://doi.org/10.1016/j.engappai.2021.104206
Received 20 June 2020; Received in revised form 21 January 2021; Accepted 14 February 2021
Available online xxxx
0952-1976/© 2021 Elsevier Ltd. All rights reserved.

determined by a combination of local resuspension, horizontal advection, and vertical settling processes (e.g., Engelund and Hansen, 1967; Weeks et al., 1993), traditional physical approaches tried to link the targeted SSC to potentially related environmental factors (e.g., Nielsen, 1992; van Rijn, 1993; Soulsby, 1997). However, due to the complicated physical interactions, process-based models may not consider all the important parameters, thus the processes involved have to be simplified, for example, by adding dummy constants for consistency or simplifying the boundary conditions for applicability (Dey et al., 2018). Besides, establishing empirical formulas for different locations via physical experiments requires considerable time and money. Although many empirical formulas have been proposed for various locations (e.g., Green and Black, 1999; Zhang et al., 2018a), it is still questionable whether the empirical formulas can be successfully applied to different regions. Consequently, while physically explicit process-based models are the ultimate goal, these models may not be available shortly due to the complexity, uncertainty, and stochastic nature of sediment movement (Shojaeezadeh et al., 2020).

In addition to physical approaches, data-driven methods (DDMs) have been introduced in recent years and proven to have higher accuracy in river SSC modeling (Nagy et al., 2002; Afan et al., 2016). Examples include artificial neural networks (ANNs) (e.g., Hamidi and Kayaalp, 2008; Bayram et al., 2012; Sari et al., 2017), adaptive network-based fuzzy inference systems (e.g., Buyukyildiz and Kumcu, 2017), support vector machine models (Lafdani et al., 2013; Himanshu et al., 2017; Yilmaz et al., 2018; Khan et al., 2019; Chen and Chau, 2019) and semiparametric approaches (Wang et al., 2011). DDMs automatically recognize the relationship between the targeted variable and the environmental predictors from a large dataset to obtain a highly accurate forecasting system (Wang and Tian, 2013; Aksoy and Mohammadi, 2016; Safari, 2019). Therefore, DDMs have become a potential tool for the design and implementation of management practices by hydraulic and environmental engineers, attracting a growing body of applications for river engineering and water resources (Bowers and Shedrow, 2000; Sharafati et al., 2019).

However, given that DDMs could achieve higher prediction accuracy than physical models (Nagy et al., 2002), they usually cannot provide sufficient explanation in physical meanings, i.e., a balance always exists between accuracy and interpretation (Doshi-Velez and Kim, 2017; Molnar, 2020). To address this issue, a more interpretable DDM, least absolute shrinkage and selection operator (LASSO) regression (Tibshirani, 1996), is introduced in the present paper for coastal SSC modeling. It is expected that the most important factors among the investigated parameters can be found through the "shrinkage" of LASSO to provide more concise but still reliable predictions. To the best of the authors' knowledge, the LASSO method has been rarely introduced for SSC modeling in coastal oceans therefore has great potential for popularization (Etheridge et al., 2014).

Considering that DDMs are promising alternatives for SSC prediction with the availability of large datasets, in situ measurements of SSC and hydrodynamics were taken in the subaqueous Yellow River Delta (YRD), China, in the winter of 2014–2015. This large dataset is employed for training and testing a LASSO regression model as well as several alternative DDMs for SSC prediction. One-order temporal autocorrelation of the residuals from the conventional LASSO is found and incorporated to form a temporal LASSO model in the present work. This processing significantly improves the forecast performance of all DDMs, because physically it means that the static settling process of suspended sediments is considered. The LASSO model outperforms the other alternative DDMs both in accuracy and interpretability either in cases with or without temporal autocorrelation. Finally, direct signal analysis of the SSC time series with empirical mode decomposition (EMD) and spectrum analysis (SA) is conducted to validate the rationality of the LASSO "shrinkage" and the physical mechanism explanation obtained from LASSO. As EMD and SA have been used in the analysis of hydrodynamics (Bian et al., 2020) and SSC data (Müller et al., 2009), these techniques provided a physical perspective for verifying the DDM results.

The structure of this paper can be outlined as (1) a background introduction to the topic, (2) the main methods employed in the present work, (3) the field data collection process and data quality control, (4) the derivation of the temporal LASSO model and comparisons with other DDMs for accuracy evaluation, and (5) discussion of the interpretability of the temporal LASSO model and verification of the rationality of the LASSO "shrinkage" (DDM perspective) with direct data analysis using EMD and SA (physical perspective).

2. Methods

The main methods employed in the present paper are briefly illustrated in this section.

2.1. LASSO regression

Introducing a penalty item in linear regression can efficiently shrink the coefficient estimates and significantly reduce a model's variance, especially in a model with high-dimension predictors (Friedman et al., 2001). The LASSO regression (Tibshirani, 1996), which incorporates a penalty item (L_1) in linear regression, can force some of the coefficient estimations to exactly equal 0 with a sufficiently large tuning parameter. This means that LASSO can automatically select the most important independent variables by shrinking the less important predictors to 0. Given a dataset (x_i, y_i) (x_i is a p-dimensional vector), the corresponding optimized objective of LASSO is formulated as:

$$\sum_{i=1}^{n}\left(y_i-\beta_0-\sum_{j=1}^{p}\beta_j x_{ij}\right)^2+\lambda\sum_{j=1}^{p}\left|\beta_j\right| \tag{1}$$

where β_0 is the shift of LASSO, β_j represents the coefficients of x_{ij}, and λ is the regularization parameter. According to the coefficient estimates from Eq. (1) with proper regularization, LASSO can produce simpler and more interpretable models by shrinking some estimates to 0. Additionally, it can significantly reduce the variance in the model (James et al., 2013).

2.2. Temporal pattern recognition

For time series analysis, the autocorrelation function (ACF) can be used to evaluate the linear relationship between the lagged values of the series. Assuming a time series $\{u_1, u_2, \ldots, u_T\}$, the ACF ρ_k is given as (Box et al., 2015):

$$\rho_k=\frac{\sum_{t=k+1}^{T}\left(u_t-\bar{u}\right)\left(u_{t-k}-\bar{u}\right)}{\sum_{t=1}^{T}\left(u_t-\bar{u}\right)^2} \tag{2}$$

where $\bar{u}$ is the mean of the time series and k is the lag order.

Based on the ACF, the partial autocorrelation function (PACF) $\varphi_k = \begin{pmatrix}\varphi_{k1} & \cdots & \varphi_{kk}\end{pmatrix}^T$ is defined as:

$$\begin{bmatrix}\varphi_{k1}\\ \varphi_{k2}\\ \vdots\\ \varphi_{kk}\end{bmatrix}=\begin{bmatrix}1 & \rho_1 & \cdots & \rho_{k-1}\\ \rho_1 & 1 & \cdots & \rho_{k-2}\\ \vdots & \vdots & & \vdots\\ \rho_{k-1} & \rho_{k-2} & \cdots & 1\end{bmatrix}^{-1}\cdot\begin{bmatrix}\rho_1\\ \rho_2\\ \vdots\\ \rho_k\end{bmatrix} \tag{3}$$

Given a time series, future observations can be predicted via a linear combination of the historical observations and the corresponding PACF values. According to the ACF and PACF values, the pattern of the time series can be detected (Metcalfe and Cowpertwait, 2009).

2.3. Empirical mode decomposition

To analyze the non-linear and non-stationary signals, Huang et al. (1998) proposed the empirical mode decomposition (EMD) method, which can decompose the original signals into several intrinsic mode functions (IMFs) and residuals that accept the Hilbert transformation. The EMD method is determined only by the pattern of the signal without any complex assumption (Wu et al., 2019). Given a signal series $Z(t)$ $(t = 1, 2, \dots, T)$, the steps of EMD can be illustrated as follows (Rilling et al., 2003):

(a) Let $X(t) = Z(t)$, and detect all the local extremes of $X(t)$.
(b) Implement the upper envelope $X_u(t)$ through a cubic spline to connect all the local maxima. Similarly, implement the lower envelope $X_l(t)$ by connecting all the local minima.
(c) Calculate the mean of envelope $M(t)$ by averaging the corresponding values from $X_u(t)$ and $X_l(t)$.
(d) Obtain the signal $X^{o}(t)$:

$$X^{o}(t) = X(t) - M(t). \tag{4}$$

If $X^{o}(t)$ is an IMF, let $C_i(t) = X^{o}(t)$. Otherwise, replace $X(t)$ by $X^{o}(t)$, and repeat steps (a)–(d) until all IMFs are achieved.
(e) Obtain the remaining signal $R(t)$:

$$R(t) = X(t) - C(t). \tag{5}$$

Let $X(t) = R(t)$, and decompose the new signal $X(t)$ by repeating steps (a)–(d) until the remaining signal is a monotone signal R_n.

Finally, following the above steps of EMD, the original signal $Z(t)$ can be represented as:

$$Z(t) = \sum_{i=1}^{n-1} C_i(t) + R_n \tag{6}$$

with n sub-signals.

3. Field dataset

A large dataset is needed to train and test the performance of the methods described in Section 2 in SSC prediction and mechanism explanation. Therefore, long-term in situ observations of coastal SSC and hydrodynamics were made in the modern YRD, China (Fig. 1), in the winter of 2014–2015. The dataset is employed in the present paper for investigation.

3.1. Study area

The modern YRD is located in the southwest of the semi-enclosed Bohai Sea, China, between Bohai Bay and Laizhou Bay (Fig. 1). The modern YRD formed after the Yellow River diverted in 1855 and began flowing into the Bohai Sea. The course of the Yellow River has changed more than 50 times in the past 166 years for reasons more anthropogenic than natural, forming several abandoned lobes. The study area (Chengdao sea) is located on the abandoned Diaokou lobe in the northern part of the YRD (Fig. 1). After the Yellow River diverted to the Qingshuigou course in 1976, the Diaokou lobe experienced strong sediment resuspension, exportation, and coastline retreat due to both the loss of riverine sediment supply and exposure to energetic northerly waves. As the second-largest oilfield in China (Shengli oilfield) is located in this region, evaluating the sediment dynamics in this area will help the relevant departments designate engineering protection measures. From a long-term perspective, accurate prediction of SSC is beneficial to the prediction of the coastline and beach evolution in this area.

The mechanisms that affect SSC changes mainly include the river input, local resuspension caused by waves or currents, settling processes (Maa and Kwon, 2007; Shao et al., 2011), and horizontal advection by tidal currents (Zhang et al., 2021). Horizontal advection is normally negligible for sands but not for fine-grained sediments (Weeks et al., 1993). There is almost no possibility of SSC changes caused by river input in the present area because the observation site (abandoned Diaokou lobe) is ~50 km from the present river mouth (Fig. 1). Additionally, the flood season of the Yellow River is from June to September (Bi et al., 2011), which corresponds to precipitation, but the observation was conducted in the winter of 2014–2015.

3.2. Data collection

An instrumented tripod platform was deployed at the seafloor of the site (38°10'15.40N, 118°54'55.37E) to synchronously measure the tide (water depth), wave, current, and water turbidity parameters from December 09, 2014, to April 22, 2015. The tripod was instrumented with one wave gauge (virtuoso, RBR, Canada), one electromagnetic current meter (JFE Infinity-EM, Alec, Japan), and one nephelometer (CTD XR-620, RBR, Canada) with a built-in optical backscatter sensor (OBS) (Fig. 2). Detailed information about the instruments, sampling settings, and elevation of the instruments on the tripod (relative to the bottom) are summarized in Table 1.

Surficial sediment samples were collected from the observation site by a diver. The grain size composition indicated that the surficial sediments were sandy silts (clay 4.72%; silt 52.66%; fine sand 42.62%) with d_{50} = 0.057 mm. The sediments were poorly sorted (δ_i = 1.26) with very positive skewness (S_{ki} = 0.32) and very leptokurtic kurtosis (K_g = 1.56).

3.3. Turbidity-SSC calibration

The direct output signal from the nephelometer was turbidity with units of NTU. A calibration was needed to transform the turbidity into SSC. Therefore, a series of water–sediment mixtures with known SSCs were prepared in the laboratory using silts collected from the field site. The nephelometer was then used to measure the corresponding turbidities. As a simple linear regression between SSC and turbidity is normally adequate (Pavanelli and Pagliarani, 2002; Zhang et al., 2018b), linear regression was performed between the measured turbidities and the corresponding SSCs. The calibration results can be found in Zhu et al. (2018). The turbidity readings from the field nephelometer were converted into SSC using the calibrated relationship.

3.4. Observational results

All the measured parameters are employed as predictors in the present work: water depth (D), significant wave height (H_s), wave period (T_s), total current speed (V), and SSC. The wind speed (V_w) during the observation was also available from the Shengli Oilfield observation station nearby. To make all the series of the same dimension as well as removing the measurement noise, all the data are averaged hourly. As the SSC is the targeted variable, it is defined as the dependent variable. All the external environmental factors are independent variables that potentially contribute to the variation in SSC. The time series of the measured predictors are shown in Fig. 3.

Fig. 3 shows that all the parameters have their periodicities, which is a clue for the characterization of their respective driving mechanisms (Table 2). The water depth shows two high and low tides each day, which is irregular semi-diurnal. The wind speed (V_w) is closely related to the wave height (H_s), indicating that the waves here are mainly wind-driven. The statistical details are summarized in Table 2.

It can be inferred from Fig. 3 that some of the independent variables (D, V_w, H_s, T_s, and V) are intrinsically related rather than mutually independent. For example, the wave parameters (H_s and T_s) are strongly related to the wind signals (V_w). More importantly, the measured flow speed (V) consists of the tidal currents and wind-driven currents because V is significantly enhanced (Fig. 3e) during wave events (Fig. 3c).

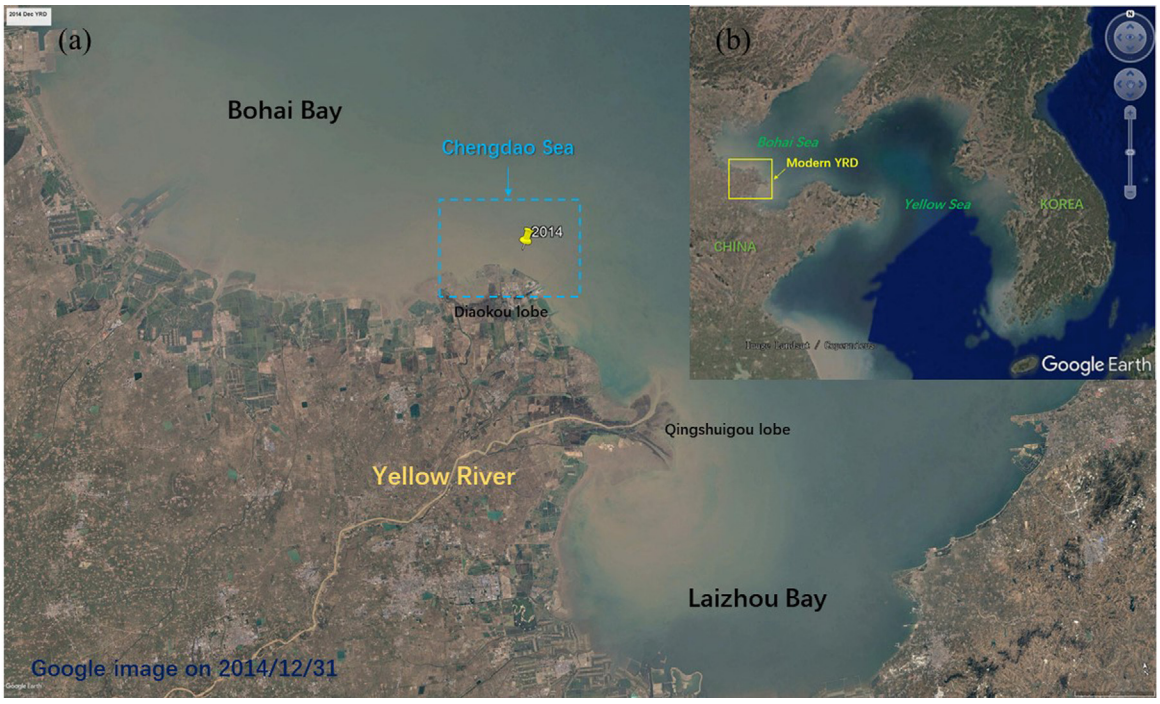

Fig. 1. Geographical location of the study area: (a) observation site (38°10′15.40″N, 118°54′55.37″E) in the Chengdao region on the abandoned Diaokou subaqueous lobe in the northern part of the modern YRD; (b) location of the modern YRD in the Bohai Sea, China.

Table 1
Observational apparatus and sampling settings.

Parameter	Manufacturer	Burst interval	Frequency	Valid time*	Elevation
Wave	RBR. Canada	5 min/1 h	6 Hz	Dec.09–Mar.30	52 cm
Current	Alec. Japan	1 min/0.5 h	1 Hz	Dec.09–Feb.07	50 cm
SSC	RBR. Canada	Continuous	Once/10 min	Dec.09–Mar.15	50 cm

* "valid time" refers to the period in which data were recorded successfully. The most comprehensive dataset, from December 10, 2014, to February 07, 2015, was analyzed in the present paper.

Table 2
Statistical details of the measurement data.

Variable	Independent variables					Dependent variable
Parameter	Water depth (D)	Wind speed (V_w)	Significant wave height (H_s)	Wave period (T_s)	Total flow speed (V)	SSC (Turbidity)
Units	m	m/s	m	s	cm/s	g/L
Maximum	7.51	18.40	3.04	12.98	80.06	3.31
Minimum	4.92	0.20	0.08	2.77	2.60	0.86
Average	6.37	5.56	0.70	5.00	21.82	1.68
Period (day)	~0.5	~2–9	~2–9	~2–9	*	**
Driving mechanism	Irregular semidiurnal tide	Atmospheric pressure	Wind-driven	Wind-driven	Tidal + wind-driven currents	Tidal and wave resuspension + tidal advection + static settling, etc.

* The period of V is more complicated than those of the other independent variables, as it is the superposition of the tidal currents (period ~0.5 days) and wind-driven currents (period ~2–9 days). ** The period of the dependent variable (SSC) is also the superposition of several periods of independent variables, which will be examined in Section 5.2.

Therefore, the respective contributions of the waves and tidal currents to the SSC cannot simply be evaluated via direct regression between the originally measured parameters, as the recorded V values are mixed with wave signals. In this case, LASSO regression is introduced and expected to realize reasonable "shrinkage" of the related factors in the present work.

4. Data modeling

To better analyze the correlation between the measured parameters and establish a predictive model, the dataset shown in Section 3 is processed with the methods from Section 2. The procedure can be outlined as follows: First, the data are interpolated to fill in the missing points due to measurement issues. Second, correlation analysis is performed for all the measured parameters, and the environmental factors are quantitatively confirmed to be interrelated. Third, conventional LASSO is employed for variable selection to infer the most important environmental factors for SSC variations. Consequently, H_s, V, and D are found to dominate the other factors, either surpassing or representing the other factors; thus, the contributions are compressed into the three dominant factors. Fourth, the residuals from LASSO are analyzed with ACF and PACF to explore the temporal pattern of the SSC series. A strong one-order autocorrelation is found in the residual. Finally, the temporal pattern is incorporated into the conventional LASSO to

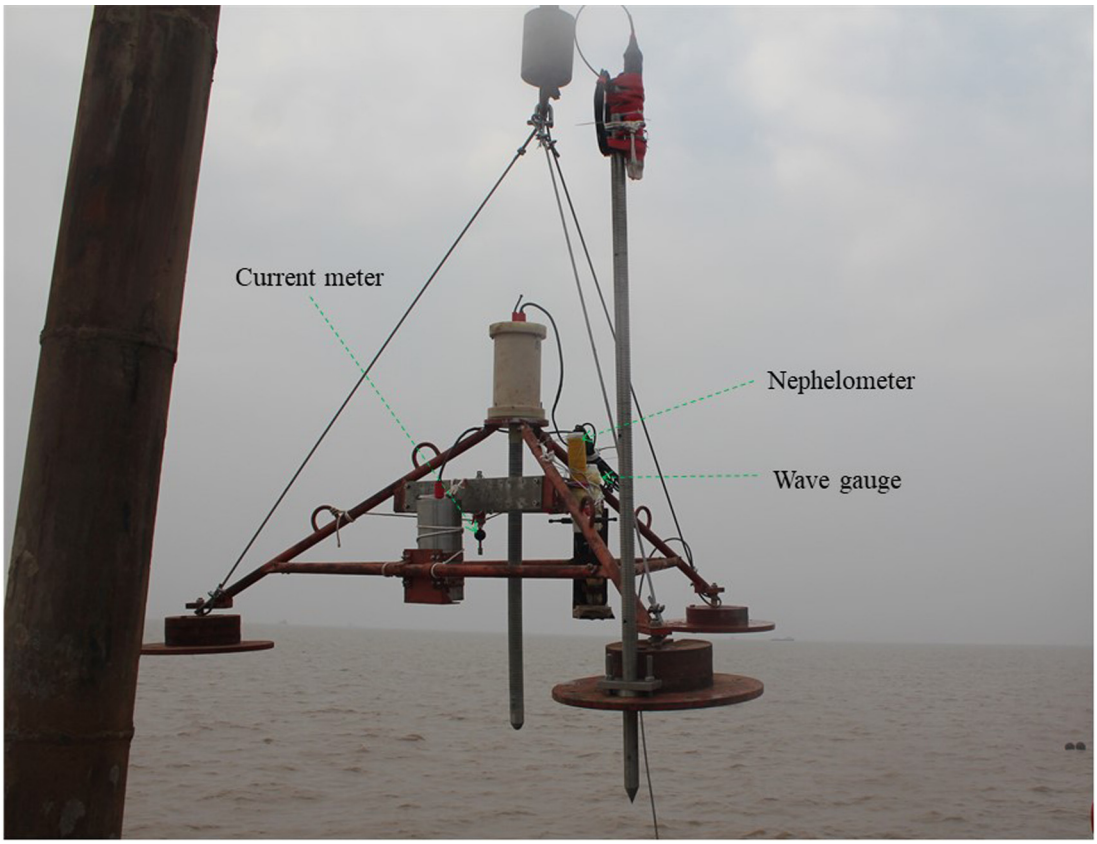

Fig. 2. Photograph of the field tripod instrumented with one wave gauge (for measuring wave height and period), one electromagnetic current meter (for measuring flow velocities), and one nephelometer (for measuring SSC).

form a new temporal LASSO model in the present paper. To test the forecasting performance of the temporal LASSO model, other three popular DDMs (support vector regression, classification and regression tree, and multilayer perception) and one statistical modeling approach (stepwise regression) are employed for comparison.

4.1. Data pre-processing

Due to instrument sampling issues, there are some missing H_s and T_s values (Fig. 3). The spline method (Perrin et al., 1987) is used to interpolate the missing points for the modeling, and the interpolated results are shown in Fig. 3 in red.

The dataset is divided into a training set from 2014/12/10 0:00 to 2015/1/26 6:00 and a test set from 2015/1/26 7:00 to 2015/2/7 3:00. The LASSO model and the other DDMs are trained with the training set, and then the performance is validated using the test set. To address interruptions from outliers in the dataset, logarithmic transformation is employed on the target (SSC) in subsequent data analysis and modeling (e.g., Wang et al., 2018).

4.2. Correlation analysis of the measured parameters

To quantitatively explore the correlation between the targeted variable and the environmental predictors, Pearson correlation coefficients are calculated and shown in Fig. 4.

As illustrated in Fig. 4a, the ln(C) has the highest correlation (0.53) with the significant wave height (H_s), which indicates that the SSC variation is dominated by wave actions (Jia et al., 2020). The ln(C) has the second-highest correlation (0.4) with the total flow speed (V), which again indicates that V and H_s are highly correlated (0.58). Moreover, the correlation coefficient (−0.16) between ln(C) and D indicates that the water depth has a negative influence on the SSC, which accords with the fact that the direct driving force for sediment resuspension (i.e., bed shear stress) is negatively related to the depth for given waves and currents (Wiberg and Sherwood, 2008). The correlation analysis results further quantitatively verify that the measured parameters are interrelated, i.e., the influence of the environmental factors can be overestimated if the signals are not decomposed or shrunk. Therefore, in the next section, LASSO is employed to better explore the role of the environmental parameters in the SSC variation mechanism and forecasting.

4.3. Estimation of coefficients with LASSO regression

Since the scales of the predictors are different, normalization is used to standardize all the investigated variables before LASSO regression. Subsequently, the regularization parameter λ is optimized as it determines the performance of LASSO (a properly large λ can efficiently shrink the coefficient estimates). 10-fold cross-validation is employed to estimate λ. In the cross-validation design, the training set is divided into 10 subsets; the process for the selection of λ is detailed in Fig. 5. According to the results of the 10 cross-validations, the best λ is estimated to be 0.0163. The coefficients estimated by LASSO with $\lambda = 0.0163$ are listed in Table 3.

As displayed in Table 3, the coefficient estimates for D, H_s, and V are −0.104, 0.163, and 0.003, respectively, while the remaining estimates are shrunk to 0. Therefore, the conventional LASSO model can be formulated as:

$$\ln C(t) = -0.104 D(t) + 0.163 H_s(t) + 0.003 V(t) + 1.002 + u(t) \quad (7)$$

where ln $C(t)$ is the logarithmic SSC, $D(t)$, $H_s(t)$, and $V(t)$ is the water depth, significant wave height, and flow velocity at moment t, respectively, $u(t)$ is the residual of LASSO. It can be noted that H_s is the most significant factor, while D is the second most important

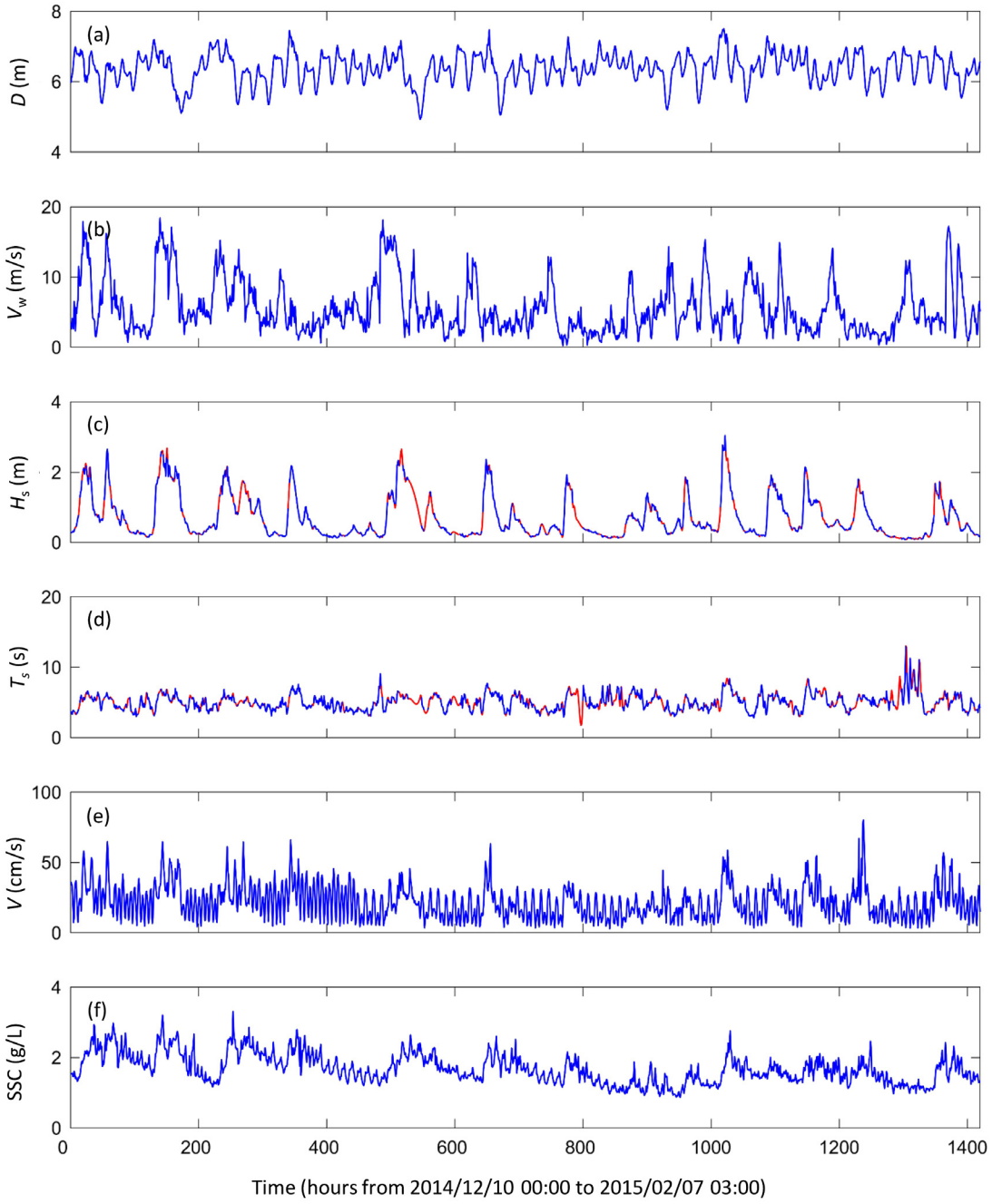

Fig. 3. Time series of the measured parameters: (a) water depth, (b) wind speed, (c) significant wave height, (d) wave period, (e) total current speed, and (f) SSC. Note: the data in red shown in (c, d) are the interpolation points (the interpolation method is detailed in Section 4.1). (For interpretation of the references to color in this figure legend, the reader is referred to the web version of this article.)

Table 3
Coefficient estimates by the conventional LASSO regression.

Term	Coefficient estimate	P-value
Intercept	1.002	0.000
D	−0.104	0.000
V_w	0	0.000
H_s	0.163	0.000
T_s	0	0.000
V	0.003	0.000

factor among all the five predictors. The contribution (coefficient) of V becomes much smaller than that shown in Fig. 4 because its influence shrinks into H_s. It seems that H_s, D, and V can efficiently represent all the environmental factors, thus making the model more concise. On the premise of accuracy assurance, the fewer parameters input into the model, the better for engineering applications, because this not only reduces the prediction cost but also avoids introducing more measurement errors.

4.4. Temporal structure modeling

Furthermore, the residuals $u(t)$ from LASSO are analyzed with ACF and PACF (Fig. 6a). It was found that the PACF cuts off after the one-order lag, while the ACF decreases gradually (Fig. 6b). Most of the residuals after the first lag are located between two bounds (the horizontal lines in Fig. 6a), indicating they have less correlation with the SSC at the targeted moment. Therefore, one-order autocorrelation

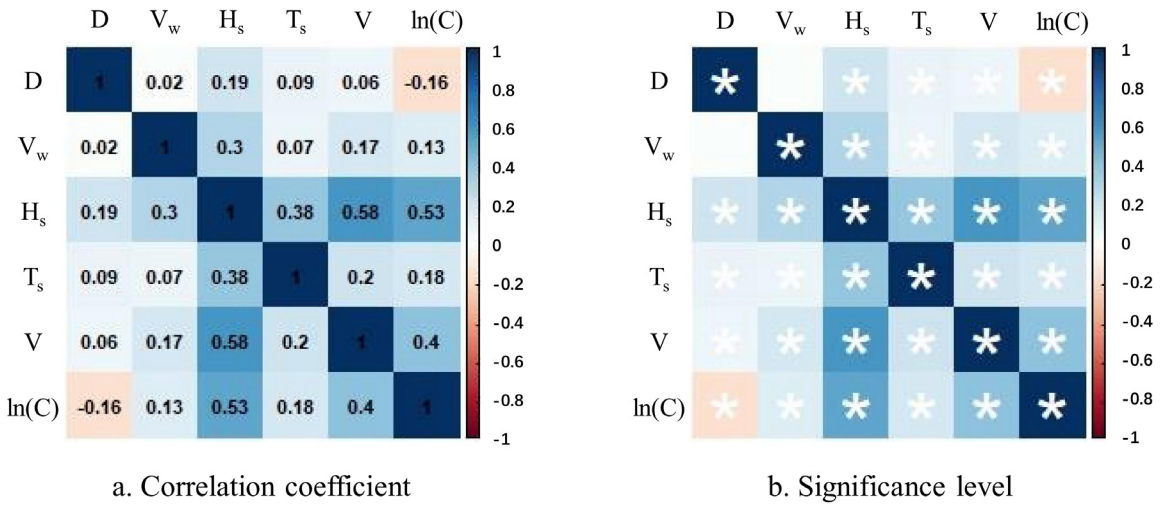

Fig. 4. Correlation analysis of the measured data: (a) correlation matrix of the Pearson correlation coefficients, and (b) significance level. Note: D is the water depth, V_w is the wind speed, H_s is the significant wave height, T_s is the wave period, V is the total flow speed and ln(C) is the SSC after logarithmic transformation.

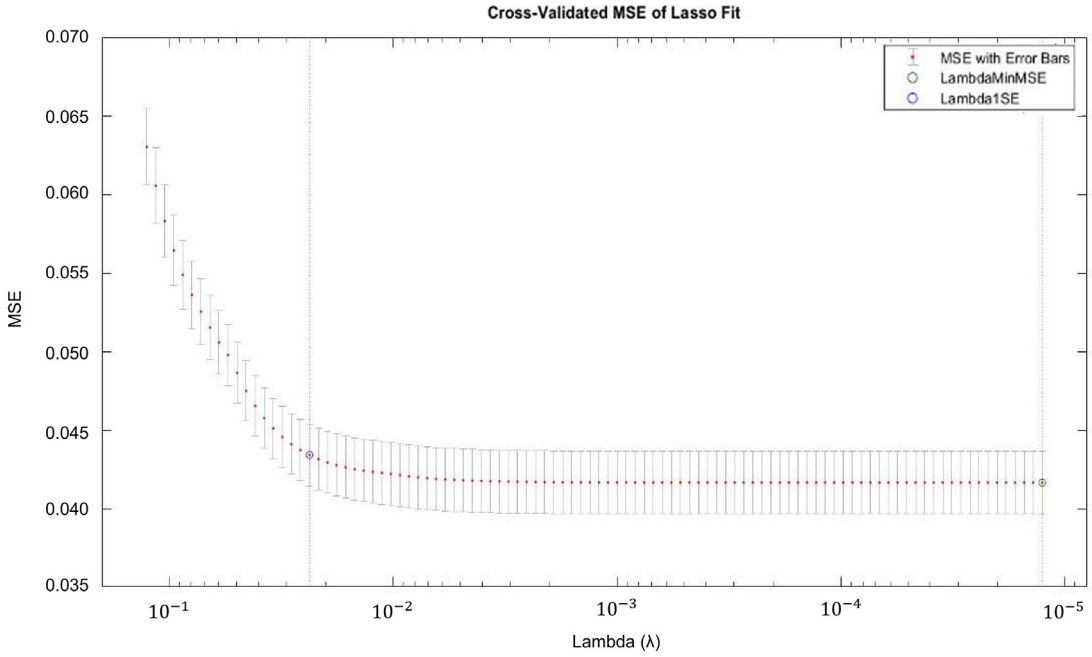

Fig. 5. The process of regularization coefficient (λ) selection using the 10 cross-validation methods in LASSO regression.

is detected from the residual of LASSO. The temporal correlation in residuals physically means that when the influence of the external environmental parameters is excluded, the present SSC(t) is still related to the adjacent historical SSC($t-1$).

According to the Akaike information criterion (AIC) (Hyndman and Athanasopoulos, 2018), the residual series follows an autoregressive model of order one, which can be formulated as:

$$u(t) = 0.888u(t-1) + \epsilon(t) \tag{8}$$

where $u(t) = \ln C(t) + 0.104D(t) - 0.163H_s(t) - 0.003V(t) - 1.002$ is the residual of LASSO at time t after the influence of environmental factors is removed and $\epsilon(t)$ is the white noise. According to the coefficient 0.888, it can be judged that the adjacent historical SSC plays a critical role in SSC modeling due to the one-order autocorrelation of the residuals. This makes sense in physics because physically it means that the information of static settling of suspended sediments in the water column is still hidden in the residual. This point will be further discussed in Section 5.1. Finally, the temporal LASSO model can be formulated as:

$$\ln C(t) = -0.104D(t) + 0.163H_s(t) + 0.003V(t) + 1.002 + 0.888u(t-1) + \epsilon(t) \tag{9}$$

where $u(t-1) = \ln C(t-1) + 0.104D(t-1) - 0.163H_s(t-1) - 0.003V(t-1) - 1.002$ in which $C(t-1)$, $D(t-1)$, $H_s(t-1)$ and $V(t-1)$ are the values measured one hour before t. Different from the existing LASSO regression models in other fields (e.g., Wang and Tian, 2013), the temporal autocorrelation pattern (Paparella et al., 2014) in the SSC time series is incorporated into the conventional LASSO model to finally form the temporal LASSO regression model in the present work.

4.5. Model performance

To test the performance of the temporal LASSO model in SSC forecasting, other three machine learning approaches, support vector

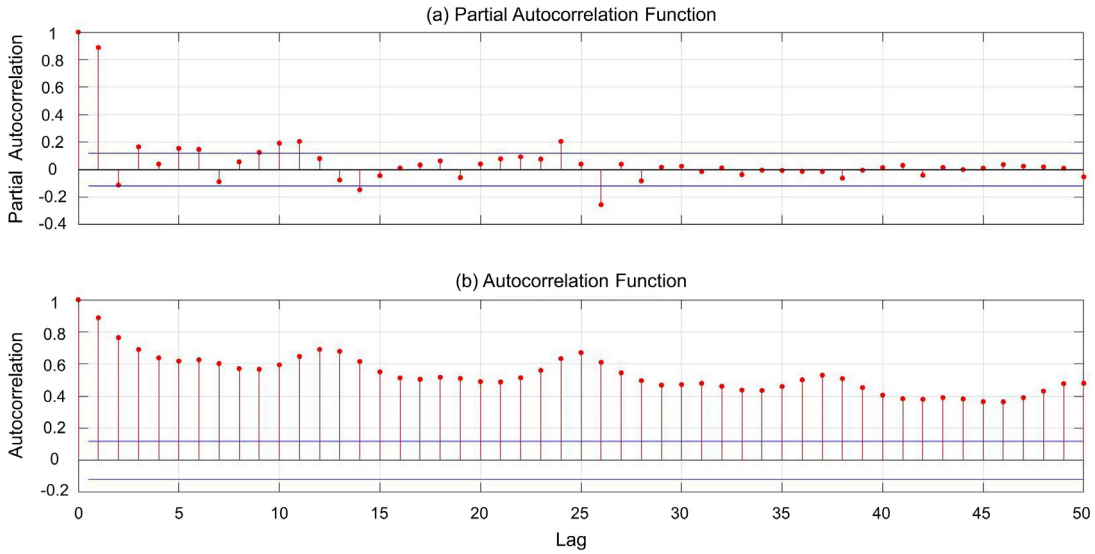

Fig. 6. Results of the temporal structure analysis with PACF and ACF for the residuals from LASSO regression. (For interpretation of the references to color in this figure legend, the reader is referred to the web version of this article.)

regression (SVR), classification and regression tree (CART), multilayer perceptron (MLP), and one statistical modeling algorithm, stepwise regression (stepwise), were employed for comparison.

All five models are investigated with and without considering the one-order temporal autocorrelation. The performance of different parameter settings in the alternative DDMs is also investigated. In SVR modeling, three basic kernel functions are used: the Gaussian kernel, linear kernel, and polynomial kernel. For CART modeling, the minimum number of branch node observations (MinParentSize) is set at 20, 30, 40, and 50. For the MLP structure, the hidden node number is fixed at 10, 15, 20, and 25. The remaining parameter settings for the alternative DDMs are as follows: SVR (regularization coefficient = 1.0, and the insensitive parameter $\varepsilon = \mathrm{IQR}(y_i)/13.49$) where IQR is the interquartile range, CART (maximum number of decision splits = 1, and minimum number of leaf node observations = 1), MLP (activation function = sigmoid function), and stepwise (tolerance for adding terms to the model = 0.05, and tolerance for removing terms from the model = 0.10). More details of the parameter settings can be found in the attached source code as **Supplementary Information**.

To evaluate the SSC forecasting performance, the root mean squared error (RMSE) and mean absolute error (MAE) are used to evaluate the error between the predictions and observations:

$$\mathrm{RMSE} = \sqrt{\frac{1}{n}\sum_{i=1}^{n}\left(y_i - \hat{y}_i\right)^2}, \tag{10}$$

and

$$\mathrm{MAE} = \frac{1}{n}\sum_{i=1}^{n}\left|y_i - \hat{y}_i\right| \tag{11}$$

where $\hat{y}_i$ is the i_{th} prediction value, y_i is the i_{th} observation value, and n is the sample size.

The SSC modeling results of all approaches are displayed in Table 4. Three interesting observations can be made. The first is that the temporal autocorrelation significantly improves the accuracy of SSC prediction for all investigated approaches (SVR, CART, MLP, stepwise, and LASSO). One of the obvious cases is that the RMSE of the MLP with 20 hidden nodes in the test set decreases from 0.204 to 0.125, while the MAE decreases from 0.166 to 0.095. Another point is that the linear relationships are more significant than the non-linear ones. In particular, in the test set, for temporal SVR modeling, the linear kernel (RMSE 0.109, MAE 0.086) is superior to the Gaussian kernel (RMSE 0.155, MAE 0.120) and polynomial kernel (RMSE 0.197, MAE 0.122). The same point can be obtained when linear modeling approaches (stepwise regression and LASSO regression) are compared with non-linear modeling approaches (CART and MLP). The last point is that the LASSO approach with/without temporal structure outperforms all investigated machine learning and statistical modeling approaches. According to Table 4, in the test set, the RMSE and MAE of LASSO without the temporal structure are 0.178 and 0.145, respectively, while those of LASSO with the temporal structure are 0.107 and 0.084, respectively. In summary, based on the model performance comparison, the temporal LASSO model is proven to be the most effective and concise tool for SSC forecasting.

Based on the performance indexes from Table 4, the models with optimal indexes (SVR model with linear kernel, CART with MinParentSize 50, and MLP with 20 hidden nodes) are further compared with the LASSO model in a Taylor diagram for both with and without the consideration of temporal structure scenarios.

As illustrated in Fig. 7, similar observations can be made. First, the LASSO approach is superior to other approaches, yielding both the smallest RMSE value and standard deviation, both in with and without the temporal autocorrelation incorporated cases. Moreover, a comparison of Fig. 7a to b shows that the SSC prediction accuracy significantly increases with the incorporation of the temporal autocorrelation structure. Again, the temporal LASSO model proposed in the present work is proven to be the most effective in SSC prediction.

5. Discussion

Now that the temporal LASSO model outperforms other alternative DDMs in terms of accuracy, it is instructive to further discuss the interpretability of the model. First, the physical meaning and the forecastability of the model are inferred from the LASSO model formula (Eq. (9)). Second, to validate the interpretation of the formula, EMD and SA are employed to analyze the mechanisms of SSC variations from a physical perspective. The quantitative contribution of each mechanism is evaluated with the ratio of variance. The results support the interpretation directly obtained from the formula; additionally, the rationality of LASSO shrinkage is also verified.

5.1. Interpretability and forecastability of the model

As the temporal LASSO model shown in Eq. (9) is a linear model, it is easy to explain its physical implications directly. The SSC at a certain

Table 4
SSC prediction performance of all the investigated models.

		Without temporal structure				With temporal structure			
		training set		test set		training set		test set	
	Parameter	RMSE	MAE	RMSE	MAE	RMSE	MAE	RMSE	MAE
SVR	"Gaussian"	0.146	0.094	0.218	0.173	0.104	0.073	0.155	0.120
	"linear"	0.204	0.158	**0.184**	**0.152**	0.098	0.075	**0.109**	**0.086**
	"polynomial"	0.193	0.146	0.251	0.179	0.103	0.079	0.197	0.122
CART	20	0.132	0.097	0.218	0.173	0.118	0.086	0.186	0.143
	30	0.147	0.111	0.218	0.170	0.125	0.092	0.186	0.141
	40	0.158	0.121	0.215	0.173	0.124	0.093	0.180	0.136
	50	0.163	0.126	**0.214**	**0.171**	0.125	0.094	**0.174**	**0.132**
MLP	"5-10-1"	0.185	0.141	0.203	0.163	0.110	0.084	0.138	0.107
	"5-15-1"	0.192	0.148	0.194	0.159	0.104	0.080	0.123	0.096
	"5-20-1"	0.190	0.148	**0.204**	**0.166**	0.101	0.078	**0.125**	**0.095**
	"5-25-1"	0.183	0.138	0.197	0.154	0.115	0.089	0.148	0.112
Stepwise regression		0.206	0.160	0.198	0.166	0.098	0.075	0.110	0.086
LASSO regression		0.206	0.162	0.178	0.145	0.095	0.072	0.107	0.084

Note: All the bold numbers are further shown in Fig. 7.

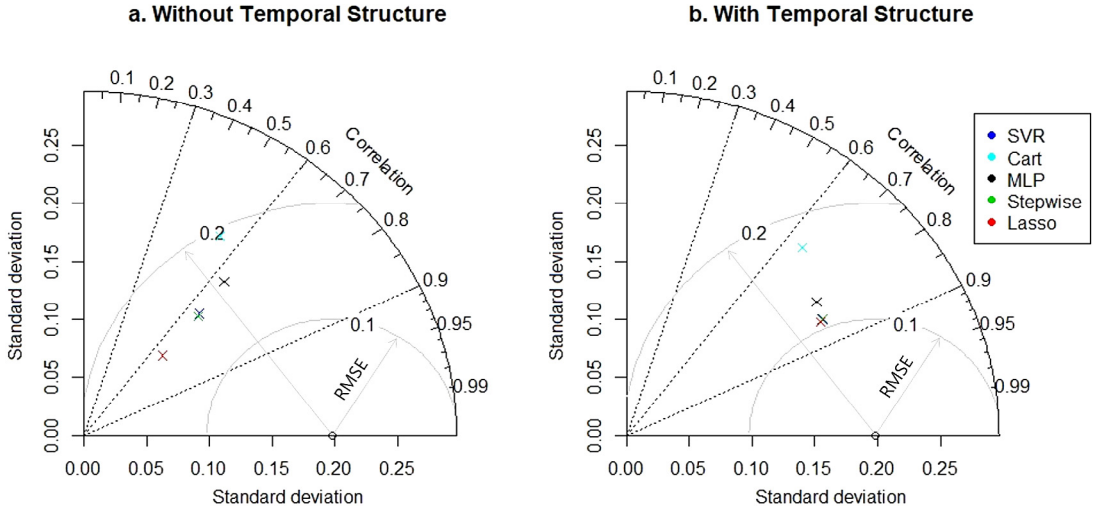

Fig. 7. Taylor diagram showing the SSC forecast performance of all the DDMs with optimal indexes in the test sets (a) without the one-order autocorrelation (b) with the temporal autocorrelation incorporated.

elevation in the water column is well known to be determined by local resuspension, horizontal advection, and downward settling (Weeks et al., 1993). In the present model, the SSC is positively related to H_s and V but negatively related to D. This makes sense because the bed shear stress which is the direct driving force for sediment resuspension is known to be positively related with H_s and V but negatively related to D. Besides, the SSC is positively related to $u(t-1) = \ln C(t-1) + 0.104D(t-1) - 0.163H_s(t-1) - 0.003V(t-1) - 1.002$, i.e., when the external disturbances are excluded, the SSC at a given moment (t) is found to be closely related to its value one hour ago at moment ($t-1$). This means that the SSC also changes even all the external environment factor values are zero (i.e., static water). Physically, this corresponds to the self-settling of suspended sediment particles in static water. More specifically, one-order autocorrelation means that within the time scale of 1 h (sample interval of the data), the SSC variation caused by static settling is relatively small compared with the changes caused by the external environmental factors (e.g., D, H_s, and V), but this is not the case for time scales longer than 2 hours (Fig. 6a). This explains why the incorporation of the one-order autocorrelation of SSC significantly improves the modeling accuracy because another important physical process (i.e., static settling) is taken into consideration. The constant item value of 1.002 also has its physical implication, i.e., as the background SSC value, but the absolute value is not exact because the SSC values are under logarithmic transformation.

It is also found that the temporal LASSO model can be used for forecasting. As the present measured SSC value $C(t)$ provides a base value for predicting the next value $C(t+1)$, then $H_s(t+1)$, $D(t+1)$, and $V(t+1)$ determine whether $C(t+1)$ increases or decreases. The model provides the possibility of using the present measured SSC value $C(t)$ to forecast the SSC value for the next hour $C(t+1)$ given that the D, H_s, and V information during the coming hour can be forecasted with high accuracy. This is possible because the pure hydrodynamic parameters in the oceans can currently be predicted with hydrodynamic models (e.g., Zanaganeh et al., 2009; Özger, 2010; Fusco and Ringwood, 2010; Almeida et al., 2015; Shi et al., 2019) with much higher accuracy than sediment transport models. Therefore, the temporal LASSO model provides a useful tool for short-period ahead SSC forecasting, which is very useful for practical applications, e.g., the emergency management of marine ranching to avoid the exposure of cultivated animals and plants to high-turbidity waters.

5.2. Verification of the interpretability with EMD

From the LASSO modeling, H_s is found to dominate the SSC variation at the observation site. However, whether this shrinkage is reasonable is discussed in this section through decoupling the SSC time series into 6 IMFs and a residual with the 'data-adaptive' EMD (Fig. 8a–g). The 6 IMFs are all zero mean series and the final residual has a monotone trend with the lowest frequency.

Spectrum analysis (SA), which can transform the time domain into the frequency domain, is applied to the decomposed time series. The dominant frequency information of each subseries reveals the physical mechanisms of the IMFs and the residual (Fig. 8h–n). Therefore, the dominant periodicity has been marked in each spectrum with corresponding physical meaning in Fig. 8. To double-check the period estimation results, a zero-crossing method is also used:

$$T = \frac{2t}{N-1} \tag{12}$$

where T is the period of the time series and t is the duration of the dataset, N is the number of zero-crossing (Huang et al., 2009). The dominant periodicities from the SA match with the periods estimated with the zero-crossing method, not exactly the same but within a reasonable range.

The period results are quite encouraging as it can be well explained with physical meanings (Table 5). The physical meaning of SubSSC_{1-2} is easy to understand as the periods are clear (unique) which well accord with the period of M4 tidal resuspension and M2 tidal advection, respectively. The physical meaning of SubSSC_{3-5} needs some explanation as the 3 subseries are all the SSC variations in response to the wind (wave) events which have uncertain periodicities within 2–9 days (cf. Table 2). That is, as the periodicity of wind (wave) events is not fixed, consequently, EMD decomposed the signals into 3 IMFs (SubSSC_{3-5}) with periods within the range (i.e., 2–9 days). This is technically not wrong but can be merged into one same physical process. The physical meaning of SubSSC_6 is a spring–neap tidal pumping of sediments (e.g., Li et al., 2016) and the residual corresponds to a seasonal variation trend. The EMD results show good interpretability in the aspect of physical meanings, which proves that the decomposition process functions well.

Once the components are successfully decomposed, it is instructive to further estimate their respective contributions, which has always been an important topic in coastal research (Ward, 1985; Guillou et al., 2017; Li et al., 2018; Andutta et al., 2019; King et al., 2019; Mulligan et al., 2019; Wen et al., 2019). The representative contribution of the components throughout the observation period is evaluated using the ratio of the subseries variance to the sum:

$$P = \frac{\mathrm{Var}(\mathrm{SubSSC}_n)}{\sum_1^6 \mathrm{Var}(\mathrm{SubSSC}_n)} * 100\% \tag{13}$$

where P is the contribution, Var is the variance, n is the number of subseries (IMFs). It is worth noting that as the seasonal trend (residual) can be taken as the background SSC, therefore, it is not considered in the contribution estimation with variance. The energy entropy of the subseries is also given to present the uncertainty of the subseries. All the related information is summarized in Table 5.

The quantitative results indicate that wave-induced sediment resuspension (63%) is the most important mechanism for SSC variation over the observation period, followed by tidal advection (14%), tidal resuspension by currents (12%), and spring–neap tidal pumping of sediments (10%). The results ultimately verify the rationality of the shrinkage in LASSO modeling, i.e., the contributions of other factors can be compressed to 0 as the role of H_s is significantly dominant (63%). Besides, in the study area, horizontal advection (14%) is found to be nearly equally as important as tidal resuspension (12%). The contribution estimation method and conclusions are useful for the analysis of coastal sediment dynamics because the practical one-dimensional vertical (1DV) SSC settling-diffusion model is valid only for scenarios where the horizontal advection contribution is small compared to the local processes (Nielsen, 1992, 2009).

5.3. Limitations and future works

Two limitations still exist in the present work. First, the dominant role of wave resuspension is confirmed qualitatively and quantitatively, however, more detailed mechanisms that how waves play such a dominant role in resuspending sediments (e.g., Zhang et al., 2017, 2018), require further investigation. Future works will focus on conducting longer-period observations with higher sampling frequency to explore the detailed mechanisms.

Second, only short-period (1 h ahead) forecasting of SSC is achieved in the present work. For two-step or more predictions, reliable corresponding estimates of all predictors are needed. More efforts can be focused on establishing a coupled model of EMD (Lahmiri, 2016; Alizadeh et al., 2017) with the LASSO regression, rather than just verify the temporal LASSO results with EMD from the physical perspective as at the present stage.

6. Conclusions

Suspended sediment concentration (SSC) is a key factor for water quality and regional sediment budget estimation, therefore, its prediction is very important in both environmental and ocean engineering. In situ long-term observations of SSC and synchronous hydrodynamics were conducted in the subaqueous Yellow River Delta (YRD), China, during the winter of 2014–2015. With the dataset, a least absolute shrinkage and selection operator (LASSO) regression model with temporal structure incorporated (temporal LASSO) is trained and tested for short-period ahead forecasting of SSC with high accuracy and good interpretability. The main conclusions can be summarized as follows:

(1) Incorporating the one-order temporal autocorrelation of SSC time series significantly improves the prediction accuracy of data-driven methods (DDMs). Among them, the LASSO model outperforms other DDMs either in with or without autocorrelation pattern scenarios.
(2) The temporal LASSO model has clear physical interpretability. SSC is positively related to significant wave height (H_s) and flow velocity (V), but negatively related to water depth (D). This is reasonable as the direct driving force for sediment resuspension, i.e., the bed shear stress has the same relationship with D, V, and H_s. Incorporating the autocorrelation of SSC physically means that the static settling of suspended sediments is considered, therefore, the prediction performance is improved.
(3) The temporal LASSO model can be used for short-period (1 h) ahead forecasting if the SSC value at the present moment is measured and the D, V, and H_s values in the next hour are accurately predicted with hydrodynamics models.

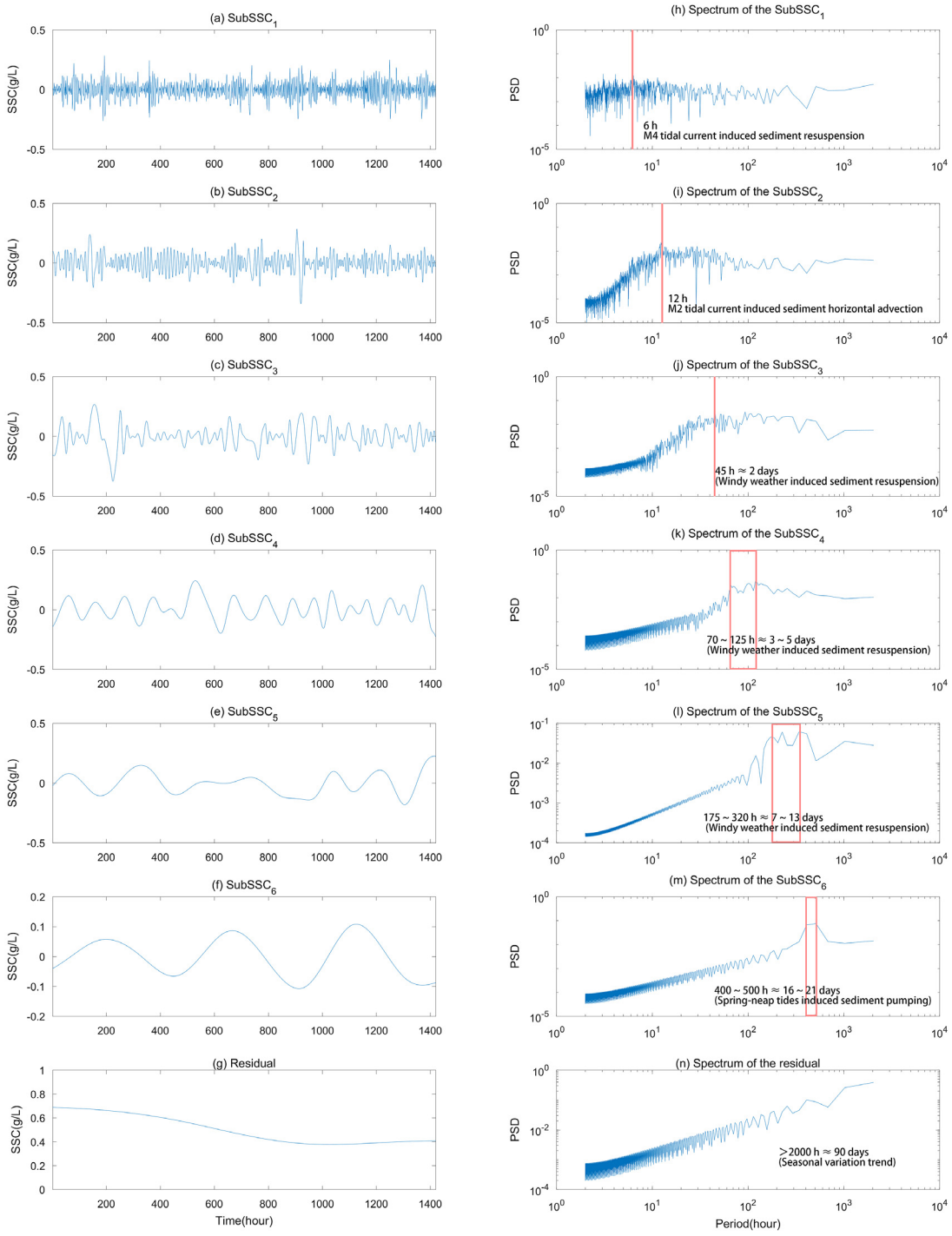

Fig. 8. EMD results of the logarithmic SSC: (a–f) $SubSSC_{1-6}$ (IMF1-6 from EMD) and (g) the residual, (h–n) corresponding spectrum of the $SubSSC_{1-6}$ and the residual. PSD is power spectrum density.

(4) Empirical mode decomposition (EMD) is employed to decouple the measured SSC and the results can be well explained with physical meanings. The contributions of each subseries (IMFs) are further evaluated via the ratio of variance. Over the observation period, M4 tidal resuspension ($SubSSC_1$) accounts for 12%, M2 tidal advection ($SubSSC_2$) accounts for 14%, sediment resuspension by waves ($SubSSC_{3-5}$) accounts for 63%, and spring–neap tidal pumping of sediments ($SubSSC_6$) accounts for 10%. The seasonal variation is reflected in the residual, acting as the background SSC therefore it is not incorporated when estimating contributions. The dominant role of waves in controlling the SSC variations identified by EMD verifies that the shrinkage of the other factors into H_s in the LASSO modeling is reasonable.

The temporal LASSO regression model proposed in the present work is shown to be a potential tool for short-period ahead SSC forecasting with high accuracy, as well as being a more interpretable way to explore the mechanisms and contributions to SSC variation in coastal oceans. Both the improvements in SSC modeling accuracy and interpretability will benefit the coastal ocean environmental engineering management.

Table 5
Key indexes and the physical explanation of the decomposed SSC time series.

	Zero-crossing no.	Zero-crossing period	Energy entropy	Variance	Contribution	Physical process
$SubSSC_1$	738	~3.85 h	1.2477	0.0047	~12%	M4 Tidal resuspension
$SubSSC_2$	269	~10.6 h	0.5790	0.0054	~14%	M2 Tidal convection
$SubSSC_3$	92	~1.3 days	0.1294	0.0083		
$SubSSC_4$	32	~3.82 days	0.0284	0.0081	~63%	Wind (wave) event-induced sediment resuspension**
$SubSSC_5$	13	~9.86 days	0.0048	0.0077		
$SubSSC_6$	6	~23.67 days	0.0013	0.0038	~10%	Spring–neap variations
Residual		~90 days	0.0000	0.0131	*	Seasonal variations

* The seasonal trend (residual) is taken as the background SSC therefore it is not considered in the contribution estimation. ** Wind (wave) event-induced sediment resuspension is not necessarily stirred up from the observation site, it could be resuspended from other source locations away from the observation site and advected to the sensor, this is another complicated topic but not the key point of the present paper and will be discussed in another paper.

CRediT authorship contribution statement

Shaotong Zhang: Conceptualization, Investigation, Data curation, Formal analysis, Visualization, Writing - original draft, Funding acquisition. **Jinran Wu:** Methodology, Software, Formal analysis, Validation, Visualization, Writing - original draft. **Yonggang Jia:** Investigation, Supervision, Funding acquisition. **You-Gan Wang:** Methodology, Software, Supervision, Writing - review & editing. **Yaqi Zhang:** Visualization, Investigation. **Qibin Duan:** Writing - review & editing.

Declaration of competing interest

The authors declare that they have no known competing financial interests or personal relationships that could have appeared to influence the work reported in this paper.

Acknowledgments

This work was supported by the Natural Science Foundation of China (grant number 41807229), the China Postdoctoral Science Foundation (grant number 2018M640656), the Natural Science Foundation of Shandong Province (grant number ZR2019BD009), Shandong Provincial Postdoctoral Program for Innovative Talents (grantee S. Zhang), the NSFC major instrument development project [grant number 41427803], and the Funding for Study Abroad Program by the Government of Shandong Province (grant number 201801026). Jinran Wu, You-Gan Wang, and Qibin Duan are supported by the Australian Research Council project (grant number DP160104292), and the Australian Research Council Centre of Excellence for Mathematical and Statistical Frontiers (ACEMS)(grant number CE140100049). Yaqi Zhang was funded by the Study Abroad Program of the Ocean University of China (grantee Y. Zhang).

The authors thank the collaborators from the First Institute of Oceanography, Ministry of Natural Resources, for their contribution to the field campaign. The postgraduate students from the Ocean University of China are thanked for the deployment and recovery of the instruments, and the laboratory experiments. The Shengli Oilfield was acknowledged for providing the wind data. We also appreciate the insightful comments from the erudite reviewers and the editor. The source code of the present work is attached as Supplementary Information.

Appendix A. Supplementary data

Supplementary material related to this article can be found online at https://doi.org/10.1016/j.engappai.2021.104206.

References

Afan, H.A., El-shafie, A., Mohtar, W.H.M.W., Yaseen, Z.M., 2016. Past, present and prospect of an Artificial Intelligence (AI) based model for sediment transport prediction. J. Hydrol. 541, 902–913.

Aksoy, H., Mohammadi, M., 2016. Artificial neural network and regression models for flow velocity at sediment incipient deposition. J. Hydrol. 541, 1420–1429.

Alizadeh, M.J., Nodoushan, E.J., Kalarestaghi, N., Chau, K.W., 2017. Toward multi-day-ahead forecasting of suspended sediment concentration using ensemble models. Environ. Sci. Pollut. Res. 24 (36), 28017–28025.

Almeida, S., Rusu, L., Guedes Soares, C., Soares, G., 2015. Application of the Ensemble Kalman Filter to a high-resolution wave forecasting model for wave height forecast in coastal areas. In: Guedes Soares, C., Santos, T.A. (Eds.), Maritime Technology and Engineering. pp. 1349–1354.

Andutta, F.P., Patterson, R.G., Wang, X.H., 2019. Monsoon driven waves superpose the effect from macro-tidal currents on sediment resuspension and distribution. Estuar. Coast. Shelf Sci. 223, 85–93.

Bayram, A., Kankal, M., Önsoy, H., 2012. Estimation of SSC from turbidity measurements using artificial neural networks. Environ. Monit. Assess. 184 (7), 4355–4365.

Bi, N., Yang, Z., Wang, H., Fan, D., Sun, X., Lei, K., 2011. Seasonal variation of suspended-sediment transport through the southern Bohai Strait. Estuar. Coast. Shelf Sci. 93 (3), 239–247.

Bian, C., Liu, X., Zhou, Z., Chen, Z., Wang, T., Gu, Y., 2020. Calculation of winds induced bottom wave orbital velocity using the empirical mode decomposition method. J. Atmos. Ocean. Technol. 37 (5), 889–900.

Bowers, J.A., Shedrow, C.B., 2000. Predicting stream water quality using artificial neural networks (ANN). WIT Trans. Ecol. Environ. 41.

Box, G.E., Jenkins, G.M., Reinsel, G.C., Ljung, G.M., 2015. Time Series Analysis: Forecasting and Control. John Wiley & and Sons.

Buyukyildiz, M., Kumcu, S.Y., 2017. An estimation of the suspended sediment load using adaptive network based fuzzy inference system, support vector machine and artificial neural network models. Water Resour. Manag. 31 (4), 1343–1359.

Chen, X.Y., Chau, K.W., 2019. Uncertainty analysis on hybrid double feedforward neural network model for sediment load estimation with LUBE method. Water Resour. Manag. 33 (10), 3563–3577.

Dey, S., Ali, S.Z., Padhi, E., 2018. Advances in analytical modeling of suspended sediment transport. J. Hydro-Environ. Res. 20, 110–126.

Doshi-Velez, F., Kim, B., 2017. Towards a rigorous science of interpretable machine learning. arXiv preprint arXiv:1702.08608.

Engelund, F., Hansen, E., 1967. A Monograph on Sediment Transport in Alluvial Streams, Vol. 10. Technical University of Denmark 0stervoldgade, Copenhagen K.

Etheridge, J.R., Birgand, F., Osborne, J.A., Osburn, C.L., Burchell, M.R., Irving, J., 2014. Using in situ ultraviolet-visual spectroscopy to measure nitrogen, carbon, phosphorus, and suspended solids concentrations at a high frequency in a brackish tidal marsh. Limnol. Oceanogr.: Methods 12 (1), 10–22.

Friedman, J., Hastie, T., Tibshirani, R., 2001. The Elements of Statistical Learning. In: Springer Series in Statistics, vol. 1, no. 10. New York.

Fusco, F., Ringwood, J.V., 2010. Short-term wave forecasting for real-time control of wave energy converters. IEEE Trans. Sustain. Energy 1 (2), 99–106.

Green, M.O., Black, K.P., 1999. Suspended-sediment reference concentration under waves: field observations and critical analysis of two predictive models. Coast. Eng. 38 (3), 115–141.

Guillou, N., Rivier, A., Chapalain, G., Gohin, F., 2017. The impact of tides and waves on near-surface SSCs in the English Channel. Oceanologia 59 (1), 28–36.

Hamidi, N., Kayaalp, N., 2008. Estimation of the amount of suspended sediment in the Tigris River using artificial neural networks. CLEAN–Soil Air Water 36 (4), 380–386.

Himanshu, S.K., Pandey, A., Yadav, B., 2017. Assessing the applicability of TMPA-3B42V7 precipitation dataset in wavelet-support vector machine approach for suspended sediment load prediction. J. Hydrol. 550, 103–117.

Huang, N.E., Shen, Z., Long, S.R., Wu, M.C., Shih, H.H., Zheng, Q., Yen, N.C., Tung, C.C., Liu, H.H., 1998. The empirical mode decomposition and the Hilbert spectrum for nonlinear and non-stationary time series analysis. Proc. R. Soc. Lond. Ser. A Math. Phys. Eng. Sci. 454 (1971), 903–995.

Huang, N.E., Wu, Z., Long, S.R., Arnold, K.C., Chen, X., Blank, K., 2009. On instantaneous frequency. Adv. Adapt. Data Anal. 1 (02), 177–229.

Hyndman, R.J., Athanasopoulos, G., 2018. Forecasting: Principles and Practice. OTexts.

James, G., Witten, D., Hastie, T., Tibshirani, R., 2013. An Introduction to Statistical Learning, Vol. 112. Springer, New York, pp. 3–7.

Jia, Y., Liu, X., Zhang, S., Shan, H., Zheng, J., 2020. Wave-Forced Sediment Erosion and Resuspension in the Yellow River Delta. Springer.

Khan, M.Y.A., Tian, F., Hasan, F., Chakrapani, G.J., 2019. Artificial neural network simulation for prediction of SSC in the River Ramganga, Ganges Basin, India. Int. J. Sediment Res. 34 (2), 95–107.
King, E.V., Conley, D.C., Masselink, G., Leonardi, N., McCarroll, R.J., Scott, T., 2019. The impact of waves and tides on residual sand transport on a sediment-poor, energetic, and macrotidal continental shelf. J. Geophys. Res.: Oceans 124 (7), 4974–6002.
Lafdani, E.K., Nia, A.M., Ahmadi, A., 2013. Daily suspended sediment load prediction using artificial neural networks and support vector machines. J. Hydrol. 478, 50–62.
Lahmiri, S., 2015. Comparing variational and empirical mode decomposition in forecasting day-ahead energy prices. IEEE Syst. J. 11 (3), 1907–1910.
Lahmiri, S., 2016. A variational mode decomposition approach for analysis and forecasting of economic and financial time series. Expert Syst. Appl. 55, 268–273.
Lambrechts, J., Humphrey, C., McKinna, L., Gourge, O., Fabricius, K.E., Mehta, A.J., et al., 2010. Importance of wave-induced bed liquefaction in the fine sediment budget of Cleveland Bay, Great Barrier Reef. Estuar. Coast. Shelf Sci. 89 (2), 154–162.
Li, Y., Jia, J., Zhu, Q., Cheng, P., Gao, S., Wang, Y.P., 2018. Differentiating the effects of advection and resuspension on SSCs in a turbid estuary. Mar. Geol. 403, 179–190.
Li, X., Zhu, J., Yuan, R., Qiu, C., Wu, H., 2016. Sediment trapping in the Changjiang Estuary: Observations in the North Passage over a spring-neap tidal cycle. Estuar. Coast. Shelf Sci. 177, 8–19.
Lloyd, D.S., 1987. Turbidity as a water quality standard for salmonid habitats in Alaska. North Am. J. Fish. Manag. 7 (1), 34–45.
Maa, J.Y., Kwon, J.I., 2007. Using ADV for cohesive sediment settling velocity measurements. Estuar. Coast. Shelf Sci. 73 (1–2), 351–354.
Metcalfe, A.V., Cowpertwait, P.S., 2009. Introductory Time Series with R. Springer-Verlag New York.
Molnar, C., 2020. Interpretable Machine Learning. Lulu.com.
Müller, J.M., Riethmüller, R., Onken, R., 2009. Multiple time scale analysis of suspended sediment concentration in the Wadden Sea. In: Coastal Engineering 2008: (In 5 Volumes). pp. 1664–1670.
Mulligan, R.P., Smith, P.C., Tao, J., Hill, P.S., 2019. Wind-wave and tidally driven sediment resuspension in a macrotidal basin. Estuar. Coasts 42 (3), 641–654.
Nagy, H.M., Watanabe, K.A.N.D., Hirano, M., 2002. Prediction of sediment load concentration in rivers using artificial neural network model. J. Hydraul. Eng. 128 (6), 588–595.
Nielsen, P., 1984. Field measurements of time-averaged suspended sediment concentrations under waves. Coast. Eng. 8 (1), 51–72.
Nielsen, P., 1992. Coastal Bottom Boundary Layers and Sediment Transport, Vol. 4. World Scientific.
Nielsen, P., 2009. Coastal and Estuarine Processes, Vol. 29. World Scientific Publishing Company.
Özger, M., 2010. Significant wave height forecasting using wavelet fuzzy logic approach. Ocean Eng. 37 (16), 1443–1451.
Paparella, F., Monk, K., Winands, V., Lopes, M.F.P., Conley, D., Ringwood, J.V., 2014. Up-wave and autoregressive methods for short-term wave forecasting for an oscillating water column. IEEE Trans. Sustain. Energy 6 (1), 171–178.
Pavanelli, D., Pagliarani, A., 2002. SW—Soil and water: Monitoring water flow, turbidity and suspended sediment load, from an apennine catchment basin, Italy. Biosyst. Eng. 83 (4), 463–468.
Perrin, F., Pernier, J., Bertnard, O., Giard, M.H., Echallier, J.F., 1987. Mapping of scalp potentials by surface spline interpolation. Electroencephalogr. Clin. Neurophysiol. 66 (1), 75–81.
van Rijn, L.C., 1993. Principles of Sediment Transport in Rivers, Estuaries and Coastal Seas, Vol. 1006. Aqua Publications, Amsterdam, pp. 11–13.
Rilling, G., Flandrin, P., Goncalves, P., 2003. On empirical mode decomposition and its algorithms. In: IEEE-EURASIP Workshop on Nonlinear Signal and Image Processing, Vol. 3, No. 3. NSIP-03. Grado (I). p. 8–11, June.
Safari, M.J.S., 2019. Decision tree (DT), generalized regression neural network (GR) and multivariate adaptive regression splines (MARS) models for sediment transport in sewer pipes. Water Sci. Technol. 79 (6), 1113–1122.
Sari, V., dos Reis Castro, N.M., Pedrollo, O.C., 2017. Estimate of SSC from monitored data of turbidity and water level using artificial neural networks. Water Resour. Manag. 31 (15), 4909–4923.
Shao, Y., Yan, Y., Maa, J.P.Y., 2011. In situ measurements of settling velocity near Baimao Shoal in Changjiang Estuary. J. Hydraul. Eng. 137 (3), 372–380.
Sharafati, A., Tafarojnoruz, A., Shourian, M., Yaseen, Z.M., 2019. Simulation of the depth scouring downstream sluice gate: The validation of newly developed data-intelligent models. J. Hydro-Environ. Res.
Shi, J., Zheng, J., Zhang, C., Joly, A., Zhang, W., Xu, P., et al., 2019. A 39-year high resolution wave hindcast for the chinese coast: Model validation and wave climate analysis. Ocean Eng. 183, 224–235.
Shojaeezadeh, S.A., Nikoo, M.R., Mirchi, A., Mallakpour, I., AghaKouchak, A., Sadegh, M., 2020. Probabilistic hazard assessment of contaminated sediment in rivers. Sci. Total Environ. 703, 134875.
Soulsby, R., 1997. Dynamics of Marine Sands. A Manual for Practical Appliations. Thomas Telford.
Taormina, R., Chau, K.W., Sethi, R., 2012. Artificial neural network simulation of hourly groundwater levels in a coastal aquifer system of the Venice lagoon. Eng. Appl. Artif. Intell. 25 (8), 1670–1676.
Tibshirani, R., 1996. Regression shrinkage and selection via the LASSO. J. R. Stat. Soc. Ser. B Stat. Methodol. 58 (1), 267–288.
Wang, Y.G., Kuhnert, P., Henderson, B., 2011. Load estimation with uncertainties from opportunistic sampling data–a semiparametric approach. J. Hydrol. 396 (1–2), 148–157.
Wang, Y.G., Tian, T., 2013. Sediment concentration prediction and statistical evaluation for annual load estimation. J. Hydrol. 482, 69–78.
Wang, N., Wang, Y.G., Hu, S., Hu, Z.H., Xu, J., Tang, H., Jin, G., 2018. Robust regression with data-dependent regularization parameters and autoregressive temporal correlations. Environ. Model. Assess. 23 (6), 779–786.
Ward, L.G., 1985. The influence of wind waves and tidal currents on sediment resuspension in Middle Chesapeake Bay. Geo-Mar. Lett. 5 (1), 71–75.
Weeks, A.R., Simpson, J.H., Bowers, D., 1993. The relationship between concentrations of suspended particulate material and tidal processes in the Irish Sea. Cont. Shelf Res. 13 (12), 1325–1334.
Wen, M., Shan, H., Zhang, S., Liu, X., Jia, Y., 2019. Contribution of waves and currents to sediment resuspension in the Yellow River Delta. Mar. Georesour. Geotechnol. 37 (1), 96–102.
Wiberg, P.L., Sherwood, C.R., 2008. Calculating wave-generated bottom orbital velocities from surface-wave parameters. Comput. Geosci. 34 (10), 1243–1262.
Wu, J., Cui, Z., Chen, Y., Kong, D., Wang, Y.G., 2019. A new hybrid model to predict the electrical load in five states of Australia. Energy 166, 598–609.
Yilmaz, B., Aras, E., Nacar, S., Kankal, M., 2018. Estimating suspended sediment load with multivariate adaptive regression spline, teaching-learning based optimization, and artificial bee colony models. Sci. Total Environ. 639, 826–840.
Zanaganeh, M., Mousavi, S.J., Shahidi, A.F.E., 2009. A hybrid genetic algorithm–adaptive network-based fuzzy inference system in prediction of wave parameters. Eng. Appl. Artif. Intell. 22 (8), 1194–1202.
Zang, Z., Xue, Z.G., Xu, K., Bentley, S.J., Chen, Q., D'Sa, E.J., et al., 2020. The role of sediment-induced light attenuation on primary production during Hurricane Gustav 2008. Biogeosci. Discuss. 1–22.
Zhang, S., Jia, Y., Wang, Z., Wen, M., Lu, F., Zhang, Y., et al., 2018a. Wave flume experiments on the contribution of seabed fluidization to sediment resuspension. Acta Oceanol. Sin. 37 (3), 80–87.
Zhang, S., Jia, Y., Wen, M., Wang, Z., Zhang, Y., Zhu, C., et al., 2017. Vertical migration of fine-grained sediments from interior to surface of seabed driven by seepage flows–'sub-bottom sediment pump action'. J. Ocean Univ. China 16 (1), 15–24.
Zhang, S., Jia, Y., Zhang, Y., Liu, X., Shan, H., 2018. In situ observations of wave pumping of sediments in the Yellow River Delta with a newly developed benthic chamber. Mar. Geophys. Res. 39 (4), 463–474.
Zhang, S., Jia, Y., Zhang, Y., Shan, H., 2018b. Influence of seepage flows on the erodibility of fluidized silty sediments: parameterization and mechanisms. J. Geophys. Res.: Oceans 123 (5), 3307–3321.
Zhang, S., Nielsen, P., Perrochet, P., Xu, B., Jia, Y., Wen, M., 2021. Derivation of settling velocity, eddy diffusivity and pick-up rate from field-measured suspended sediment concentration profiles in the horizontally uniform but vertically unsteady scenario. Appl. Ocean Res. 107, 102485.
Zhu, C., Liu, X., Shan, H., Zhang, H., Shen, Z., Zhang, B., Jia, Y., 2018. Properties of suspended sediment concentrations in the Yellow River delta based on observation. Mar. Georesour. Geotechnol. 36 (1), 139–149.